Early last glacial intra-interstadial climate variability recorded in a Sardinian speleothem

Andrea Columbu[a*], Russell Drysdale[a,b], Emilie Capron[c,d], Jon Woodhead[e], Jo De Waele[f], Laura Sanna[g], John Hellstrom[e], Petra Bajo[a]

[a] School of Geography, University of Melbourne, 221 Bouverie street, 3010, Melbourne, Australia acolumbu@student.unimelb.edu.au andrea.columbu@libero.it rnd@unimelb.edu.au p.bajo@student.unimelb.edu.au

[b] Laboratoire EDYTEM, UMR CNRS 5204, Universite deSavoie Mont Blanc, 73376 Le Bourget du Lac cedex, France

[c] Center for Ice and Climate, Niels Bohr Institute, University of Copenhagen, Juliane Maries Vej 30, 2100 Copenhagen Ø, Denmark

[d] British Antarctic Survey, High Cross Madingley Road, Cambridge CB3 0ET, UK capron@nbi.ku.dk

[e] School of Earth Sciences, University of Melbourne, Corner Swanston & Elgin streets, 3010, Melbourne, Australia jdwood@unimelb.edu.au j.hellstrom@unimelb.edu.au

[f] Department of Biological, Geological and Environmental Sciences, University of Bologna, Via Zamboni 67, 40127 Bologna, Italy jo.dewaele@unibo.it

[g] Institute of Biometeorology, National Research Council, Traversa la Crucca 3, 07100 Li Punti, Italy speleokikers@tiscali.it

*Corresponding author

Keywords: speleothems, Greenland interstadials/stadials, ice-core chronology, U-Th dating

Abstract

Chemical and physical proxy data from a precisely dated early last glacial (~113-110 ka, MIS5d) Sardinian stalagmite reveal a sub-millennial-scale, cool-dry climate event centered at 112.0 $^{+0.52}/_{-0.59}$ ka, followed by a rapid return to warm-

wet conditions at $111.76\ ^{+0.43}/_{-0.45}$ ka. Comparison with regional speleothem records and the palaeotemperature proxy record from the NGRIP ice core (Greenland) suggests that this event corresponds to Greenland Interstadial (GI) 25b and 25a, an intra-interstadial climate oscillation within GI-25, according to the recent Greenland stratigraphic framework. The speleothem age is in reasonable agreement (within 0.8 kyr) with that of the corresponding event in Greenland based on the GICC05modelext ice chronology but is older by about 3.7 kyr than the Greenland age based on the AICC2012 chronology.

1. Introduction

The transition from the Last Interglacial to the last glacial period occurred between ~120 and 110 ka, and saw the establishment of large-scale, inter-hemispheric, millennial-scale climate oscillations first documented in polar ice cores (Dansgaard et al., 1993; Grootes et al., 1993; GRIP community members 1993; NGRIP project members 2004). These abrupt climate changes, also uncovered in marine and other terrestrial archives (Voelker, 2002 and references therein) and referred to as Dansgaard-Oeschger (DO) events, persisted through the entire last glacial period. Classically, a DO event in Greenland commences with an abrupt warming of 8-16°C within a few decades (Kindler et al., 2014, and references therein). Following peak interstadial conditions (a warm phase, denoted GI for Greenland Interstadial), the climate at first gradually cools, and the end of the event is usually marked by a rapid cooling towards a relatively stable cold phase, called a Greenland stadial (GS).

Recently, significant and rapid warm-cold excursions within single, classical GI-GS succession have been reported in Greenland ice cores (Capron et al., 2010, 2012; Rasmussen et al., 2014). Such intra-GI/GS events have also been observed in Alpine cave records (Boch et al., 2011) and in southern Italian lacustrine sediments (Martin-Puertas et al., 2014) but, as yet, no further information is available for the Mediterranean region, where many existing palaeoclimate records lack sufficient resolution to detect them or have imprecise chronologies (Moreno et al., 2014). To further constrain the timing and spatial extent of millennial and sub-millennial scale climatic variability, high-resolution records are required from both near- and far-field regions so that the teleconnections, the underlying causes and the mechanisms at play can be deciphered (e.g. Banderas et al., 2012; Dokken et al., 2013; Zhang et al., 2014).

The development of robust absolute chronologies for different archives is critical in order to temporally link individual climatic events across space and to determine phase relationships between different parts of the climate system. It is difficult to obtain accurate absolute dating of Greenland ice cores once annual layer counting becomes impossible. The extension of the annual-layer-counted GICC05 chronology for the NGRIP ice core from Greenland for 0 - 60 ka (Svensson et al., 2008) is currently facilitated by two chronologies: GICC05modelext, based solely on ice-flow modeling (Wolff et al., 2010), and AICC2012, which was produced using a Bayesian tool that integrates glaciological constraints and stratigraphic markers from NGRIP and four ice cores from Antarctica (EDC, EDML, TALDICE and Vostok; Bazin et al., 2013, Veres et al., 2013). Over the glacial inception, there are discrepancies of several thousand years between the two chronologies (Veres et al., 2013; Govin et al., 2015).

A potential strategy to improve ice-core chronologies lies in the use of archives that not only preserve evidence of millennial climate events but are suited to radiometric dating with high precision. Speleothems are arguably the best-placed archives to assume this role (Henderson, 2006). Numerous speleothem records of millennial-scale climate events have emerged recently (Wang et al., 2001; Genty et al., 2003; Drysdale et al., 2007; Fleitmann et al., 2009; Boch et al., 2011), yet rigorous chronological investigations are still lacking to confidently use their absolute-dated chronologies to anchor ice-core age models. This is due in part to concerns as to whether the teleconnections between the cave and ice-core sites are persistent in time and sufficiently close in phasing, and whether the interpretation of the climate-proxy signature in the speleothem (usually calcite oxygen isotopes, $\delta^{18}O$) is robust. The chronology of the WAIS Divide ice core is currently anchored by dates from Hulu Cave (China) speleothems (Buizert et al., 2015; WAIS, 2015) but the veracity of such far-field teleconnections, especially regarding leads and lags between the abrupt warming in Greenland (identified as a rapid ice $\delta^{18}O$ increase) and the abrupt increase in monsoon intensity (based on speleothem $\delta^{18}O$), has yet to be tested.

In this paper we use oxygen ($\delta^{18}O_c$) and carbon ($\delta^{13}C_c$) isotope, petrographic and layer-morphology data from a radiometric-dated stalagmite (BMS1) from Bue Marino cave, eastern Sardinia (Suppl. Info, S.I.), to document intra-GI/GS climate oscillations during GI-25 (GI-25a-b-c: Rasmussen et al., 2014). The chronology is based on 23 U-Th ages, which were determined by multi-collector ICP-MS (Hellstrom, 2003; Drysdale et al., 2012) (see S.I.). Stable isotope samples (n=295) were measured on an AP2003 continuous-flow isotope ratio mass spectrometer following the method of Drysdale et al. (2009, S.I.). Petrographic analysis was based on the principles and nomenclature of Frisia (2015) (see S.I.). The measurements are anchored to an age-depth model constructed using the well-established finite-growth-rate technique (Drysdale et al., 2005; Scholz et al., 2012). We compare our timeseries to existing data from Western Europe and explore the chronological implications of this composite dataset in the light of the GICC05modelext (Wolff et al., 2010) and the AICC2012 (Veres et al., 2013) chronologies currently employed for the NGRIP ice core.

2. Results

The age model reveals that BMS1 grew from 112.97 $^{+0.72}/_{-0.46}$ to 110.27 $^{+0.61}/_{-0.85}$ ka (Table 1 and Fig. 1). The average 2σ uncertainty through the whole record is

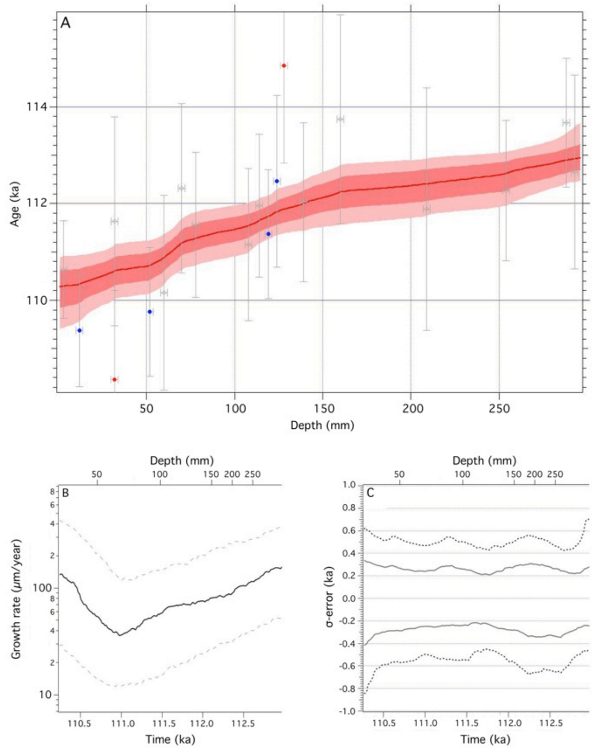

Figure 1. Age-depth model for BMS1 (a), the derived growth-rate time series (b – dotted line is 1σ error) and the propagation of the σ-uncertainty through the record (c – straight line is 1σ, dotted line 2σ). Red dots in (a) identify outliers, blue dots averaged ages (see sup. Info and Table 1). Depths are measured from the top of the stalagmite.

+0.52/-0.59 kyrs. After exclusion of two outliers from the age-depth sequence (see S.I. for discussion), the remaining ages are clearly in correct stratigraphic order within their respective age uncertainties. The growth rate varies from ~40 to ~150 μm/year, with the highest rate at the top and the base of the stalagmite. A hiatus (H) is visible at 121.5 mm from the top, at 111.76 $^{+0.43}/_{-0.45}$ ka.

The $\delta^{18}O_c$ and $\delta^{13}C_c$ variations show two distinctive intervals of progressive isotopic enrichment separated by a sharp decrease (Fig. 2). The first enrichment episode occurs from the bottom of BMS1 to the hiatus, whilst the second occurs from just after the hiatus to the top of the stalagmite (Fig. 2). The marked isotopic decrease at 111.76 ka (~1‰ for $\delta^{18}O_c$ and ~5‰ for $\delta^{13}C_c$) is the most prominent feature of this record (Fig. 3 and 4). The age-depth model cannot

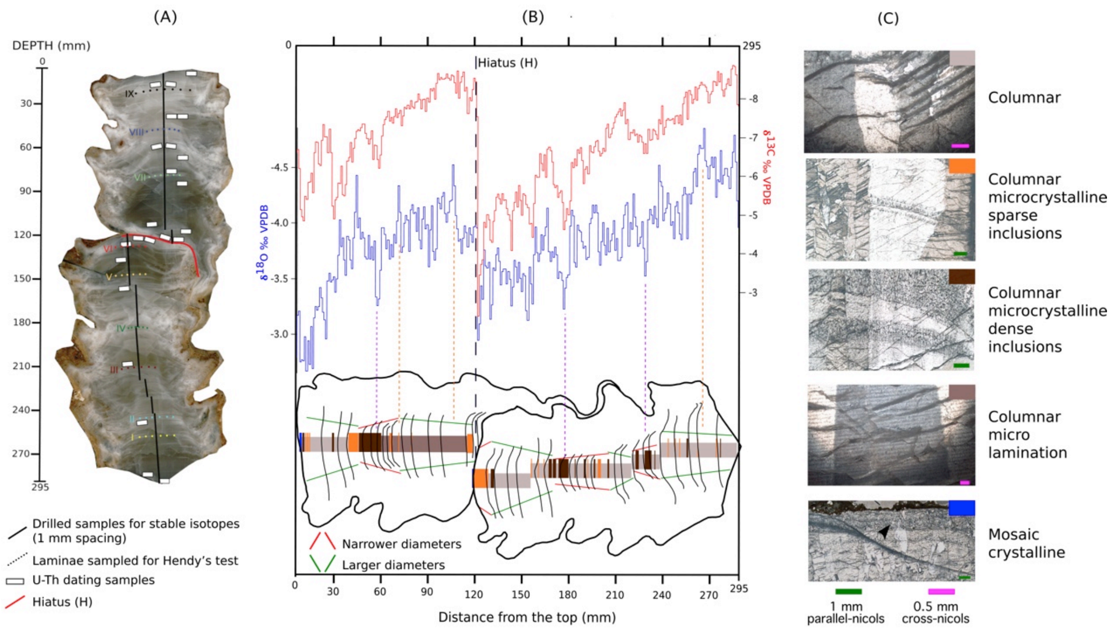

Figure 2 A) BMS1 polished surface and sampling locations for U-Th and stable isotope analyses. For the Hendy test refer to the supplementary material. B) BMS1 $\delta^{18}O$ and $\delta^{13}C$ signature compared with the micro-petrographic log and layer morphology changes (black thick line outlines the contour of the stalagmite, whilst thin black lines represent the most visible layers). Orange dotted lines highlight the principal negative isotopic excursions, most of which are correlated with columnar, detritus-poor facies (gray shading), and the widening of the growth layers. Dotted purple lines represent the principal isotopic enrichment events, correlated mostly with microcrystalline, detritus-rich facies (brown shadings) and the narrowing of the growth layers. See also the supplementary information. C) Micropetrographic facies and relative pictures. Colored boxes identified the symbols used for the micro-petrographic facies.

resolve the duration of the hiatus, suggesting that this pause in growth was of short duration.

The petrography and morphology of the speleothem correlate with the high-frequency variations in stable isotopes. Detritus-rich microcrystalline facies and narrow stalagmite diameters are associated with higher isotope ratios (50, 180 and 230 mm from the top (Fig. 2), while lower ratios mainly coincide with a columnar, detritus-free fabric and a larger stalagmite diameter (70, 110 and 270 mm from the top).

3. Discussion and concluding remarks

The calcite of BMS1 was deposited under ~equilibrium conditions, as established by Hendy test (Hendy, 1971) and petrographic analysis (see S.I.). Hence, the stable isotopes should largely reflect the original isotopic composition of the infiltrating water (Hendy, 1971; McDermott 2004). The $\delta^{18}O$ signature in the infiltrating water is mainly controlled by changes in the isotopic composition of the precipitation reaching the cave site (Fairchild et al., 2006), which is in turn affected by changes in temperature, rainfall amount (amount effect), rainfall seasonality and source (Lachniet, 2009). In terms of the amount effect, higher rainfall amounts can result in lower $\delta^{18}O$ values (Dansgaard, 1964), while higher $\delta^{18}O$ values reflect a decrease. Changes in moisture source and air-mass trajectories can also affect oxygen isotopes (Krklec & Domínguez-Villar, 2014); however, BMS1 proxies indicate the predominance of hydrological processes in driving the isotopic composition of water; in the case of a source effect, $\delta^{13}C$ should be unaffected, yet it shows a similar pattern to $\delta^{18}O$. In fact, speleothem δ^{13}C responds inversely to rainfall amount because periods of enhanced rainfall intensify soil activity, which in turn releases more isotopically depleted biogenic CO_2 and *vice versa* (Genty et al., 2003). Reduced infiltration can also result in partial dewatering of the vadose zone, exposing air-filled voids into which CO2 from percolation waters can degas, whilst lower drip rates normally associated with such a decrease can also enhance CO2 removal on the stalactite tip feeding a stalagmite. In both cases, CO2 removal preferentially releases 12CO2, leading to enriched drip water δ13C values, which in turn are inscribed as higher δ13C values in speleothem calcite (Dulinski & Rozanski 1990). The δ18O and δ13C of speleothems from sites nearby have been demonstrated to be sensitive to past variations in rainfall amount (Drysdale et al., 2006; 2009; Regattieri et al., 2014). Comparisons between the speleothem morphology, fabric and the stable isotope record together point to rainfall amount variations as the driving force behind the BMS1 isotopic signal (Fig. 2). Slower drip rates promote higher speleothem δ^{13}C (Mühlinghaus et al., 2009; Deininger et al., 2012), and also cause diametric reductions in a stalagmite (Franke, 1965; Kaufmann and Dreybrodt, 2004; Culver and White, 2005). Smaller diameters also appear connected to the pervasiveness of well-sorted detrital particles in the columnar carbonate fabric. Airborne detritus is electrostatically attracted to the humid, uppermost surface of the stalagmite and incorporated in the carbonate lattice (Dredge et al., 2013); its preservation requires a moderate-to-low drip rate because intense dripping would rework this sediment. Lower isotopic values are instead correlated to BMS1 diameter enlargement and detritus-free columnar facies, which supports the idea of enhanced drip water driven by increased rainfall. The hiatus, located at the termination of the most prominent δ^{18}O and δ^{13}C enrichment trend, represents a reduction/cessation of infiltration water triggered by a gradual rainfall decrease, as testified by the direction of the isotopic shift. However, the age model is incapable of resolving the duration of the hiatus, meaning that the period of non-deposition was relatively short (i.e. <450 years, considering 2σ uncertainty around the hiatus). In contrast, modeled growth-rate (Fig. 1) appears somewhat decoupled from the $\delta^{18}O$ and$\delta^{13}C$ patterns, particularly after the hiatus when one might expect a growth-rate increase. This could be explained by the post-hiatus translocation of the dripping point, which would have led to asymmetric growth as drip-water flow and thus calcite deposition would have been biased towards one side of the stalagmite until the equilibrium stalagmite form was re-established.

We interpret the climate information recorded in BMS1 as recording a cool-dry to warm-wet oscillation associated with the intra-GI/GS events GI-25a-b-c for three main reasons. First, the rapid $\delta^{18}O$ and $\delta^{13}C$ shift at $111.76\ ^{+0.43}/_{-0.45}$ ka is within error of the age reported for the same event in the NGRIP ice core based on the GICC05modelext (110.96 ± 1.03 ka) chronology (Wolff et al., 2010). Second, the timing agrees with similar changes attributed to the same event recorded in the NALPS speleothem record at 111.84 ± 0.63 ka (Boch et al., 2011) (Fig. 3). Finally, the shape of the event shows a striking similarity to the GI-25a-b-c sequence revealed in the NGRIP ice $\delta^{18}O$ record (Fig. 4). The shape of the GI-25a/GI-25b transition also appears similar to the other records, even taking into account the presence of the hiatus, considering its relatively short duration. Although $\delta^{18}O$ and $\delta^{13}C$ oscillations appear synchronous throughout most of BMS1 record, discrepancies are visible at the GI-25a inception (Fig. 4), just after the hiatus. This may be due to sensitivity to renewed growth after the hiatus that

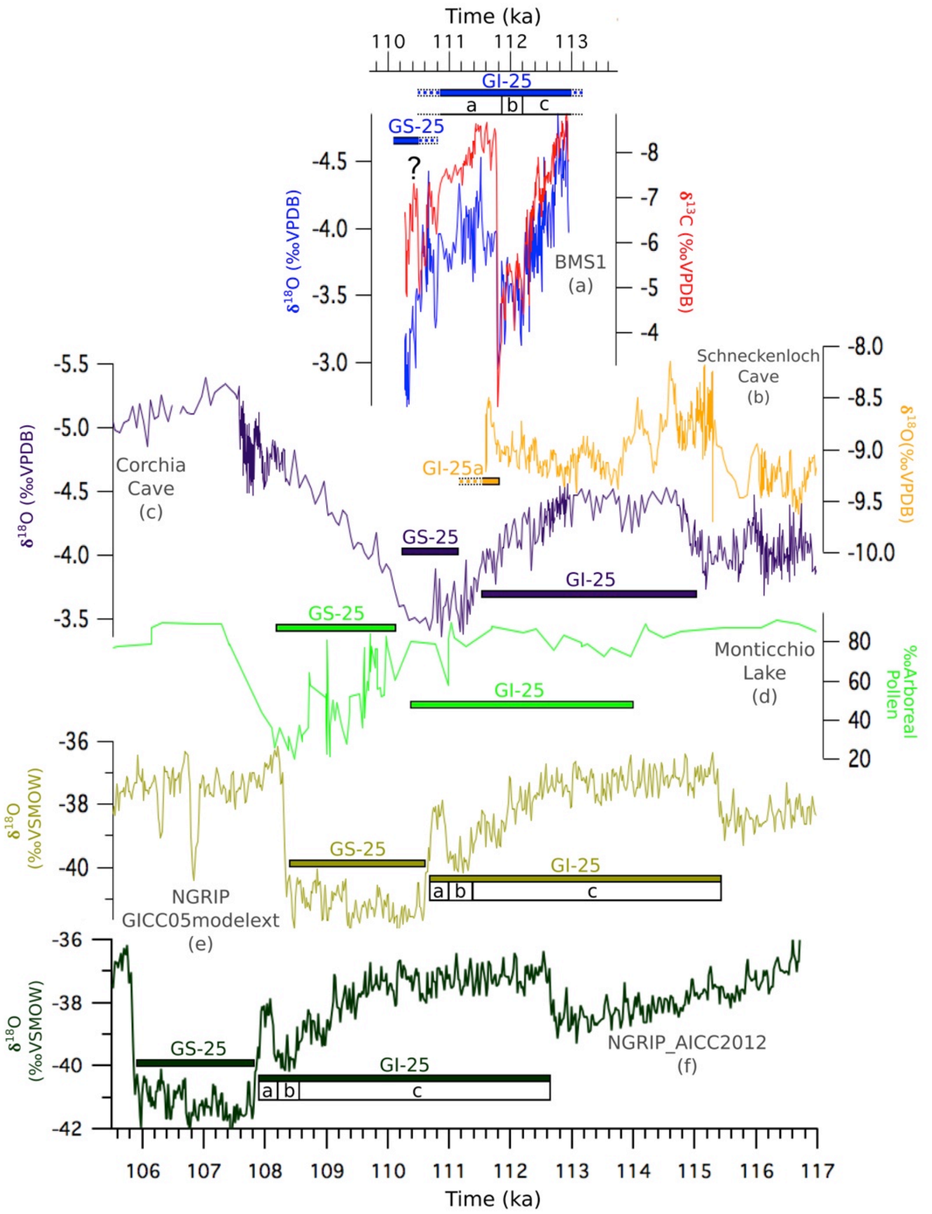

Figure 3. From top to bottom: a) BMS1 δ18O (blue line) and δ13C (red line), b) Schneckenloch (Boch et al., 2011) and c) Corchia (Drysdale et al., 2007) speleothem δ18O, d) Monticchio lake percentage of arboreal pollen (Allen and Huntley, 2009), e) NGRIP ice δ18O displayed on the GICC05modelext chronology (Wolff et al., 2010) and f) NGRIP ice δ18O displayed on the AICC2012 chronology (Veres et al., 2013). GI/GS boundaries and GI-25 subdivision (if identified) are reported with horizontal bars.

is different from one tracer to the other, as observed in a Corchia Cave speleothem record covering the early last glacial period (Drysdale et al., 2007).

GI-25a constitutes the earliest glacial “rebound-type event”, described as a short-lived warm-wet reversal during the cooling limb of a larger GI event (Capron et al., 2010, 2012), followed by a rapid return to cooler-drier conditions. At Mediterranean latitudes, such a rebound effect probably influenced the atmospheric moisture availability, whereas in continental Europe and the high latitudes of Greenland, the change was likely to be expressed predominantly as a temperature increase. Therefore, we propose that BMS1 captures an abrupt rainfall oscillation during MIS5d in the western Mediterranean region in relation with rapid climatic changes occurring during GI-25 in Greenland. GI-25a in BMS1 reported an average length of $1.08\ ^{+0.85}/_{-0.63}$ kyrs, calculated for the beginning and end of the event directly from the Monte Carlo- age simulations. Although in NGRIP record appears much shorter (~0.40 kyr), errors affecting both chronologies preclude reliable comparisons. Moreover, the premature growth interruption in the NALPS speleothem record makes calculation of the duration of the GI-25a interval in this archive difficult (Fig. 4).

The abovementioned good chronological agreement for the timing of GI-25a between the BMS1 isotopic time series and NGRIP $\delta^{18}O_{ice}$ on GICC05modelext is also seen over the GI23-GI25 sequence between the NALPS record and NGRIP on GICC05modelext (Boch et al., 2011, Veres et al., 2013). However, a discrepancy of 3.7 kyr exists for the onset of GI-25a between BMS1 and NGRIP $\delta^{18}O_{ice}$ on AICC2012 (GI-25a is recorded at ~108.1 ± 1.6 ka in AICC2012, Fig. 3). Such a discrepancy is outside the age uncertainties associated with the chronologies of both records. A large offset has already been reported for this time interval between the NALPS speleothem record and NGRIP $\delta^{18}O_{ice}$ on AICC2012 (Boch et al., 2011; Veres et al., 2013). An incongruence between AICC2012 and two other Western Mediterranean chronologies is also observed during MIS5d, i.e. the

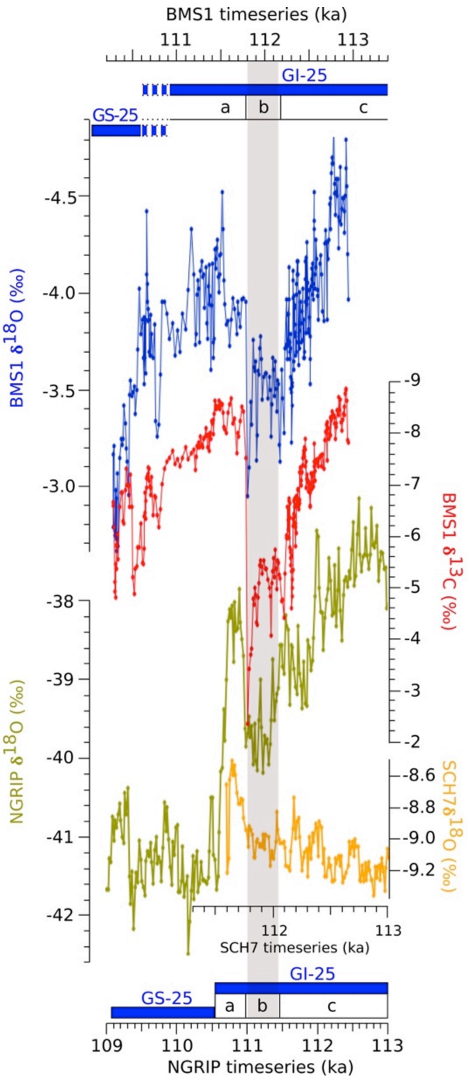

Figure 4. Similar shape between the intra-GI 25 events (GI-25a, b and c (Rasmussen et al., 2014)) in the NGRIP $\delta^{18}O$ displayed on GICC05modelext (green line) BMS1 $\delta^{18}O$ (blue line) and $\delta^{13}C$ (red line) and SCH7 (Schneckenloch cave, NALPS, orange line) records displayed on their model. The records are shifted so the onset of GI-25a in all timeseries is aligned. The GI-25a warm-wet excursion appears longer in BMS1 than in NGRIP, according to the average age model. GI-25b (gray shadow) is not represented in SCH7. Moreover, the end of SCH7 deposition at ~111.6 ka makes the definition of the length of the event in this record unclear.

Corchia speleothem (Drysdale et al., 2007) and the Lago di Monticchio (Allen and Huntley, 2009, Martin-Puertas et al., 2014), two sites located on the Italian peninsula, and dated respectively with U-Th and a combination of varve counting, accumulation rate and tephrochronology (Fig. 3). While the Corchia $\delta^{18}O$ and the Lago di Monticchio arboreal pollen percentage do not preserve convincing evidence of the intra-GI event displayed in BMS1, GS-25 can be clearly identified (Fig. 3). Its age of 111.10±1.11 ka in Corchia is clearly at odds with the start of GS-25 in NGRIP $\delta^{18}O_{ice}$ on AICC2012 (107.7±1.6 ka). Although associated with a large uncertainty, the Lago di Monticchio record also points towards an age in disagreement with the AICC2012 chronology for the GS-25 onset (110.4±5.5 ka, Martin-Puertas et al., 2014). The inaccuracy of AICC2012 during the glacial inception originates from the fact that this time interval is mostly constrained by only a few orbital markers associated with an uncertainty of up to 6 kyr (Veres et al., 2013). Our results provide new clues on the regional extension of the sub-millennial scale climatic variability and further confirmation for strong links between abrupt climate changes affecting Greenland, the Alps and the Mediterranean region during the early part of the last glacial period. However, the complete comprehension of these climate phenomena and their propagation beyond the North Atlantic/European region is only possible once precise age control is available for the different records. In this context our results suggest that the GICC05modelext chronology is more consistent with absolute chronologies of the Mediterranean-Alpine records compared to AICC2012. Nevertheless, observed differences in terms of timing, duration and shape of events between Greenland, speleothem and lake records require further high-resolution and well-dated records as well as investigations of the regional influence on larger-scale climate changes.

Assuming that a full assessment of the degree of synchronicity between climatic variability recorded in ice cores and speleothems over, for example, glacial terminations and GI onsets, can be achieved, speleothem chronologies should offer useful anchors to improve ice-core age models, especially over intervals where annual layer counting techniques are no longer applicable.

Acknowledgements

We are grateful to Salvatore Cabras for his help during the fieldwork and the staff of the Bue Marino cave for the access to the cave. This project has received funding from the European Union's Seventh Framework Programme for research and innovation under the Marie Skłodowska-Curie grant agreement no 600207.

Sample ID	Depth (mm)	^{238}U (ppb)	$(^{234}U/^{238}U)_A \pm 2\sigma$	$(^{230}Th/^{238}U)_A \pm 2\sigma$	$(^{230}Th/^{232}Th)_A$	Age uncorrected (ka)	Age corrected (ka) ±2σ	Averaged ages (ka) & outliers	2σ error (%)
BMS1-4	3	34	1.166 ± 0.003	0.759 ± 0.004	233.4	110.71	**110.64 ± 1.00**	**Age ok**	**0.91**
BMS1-2015-3a	12	96	1.160 ± 0.005	0.753 ± 0.006	236.1	110.18	**110.12 ± 1.67**	**109.37 ± 1.16**	**1.06**
BMS1-2015-3b	12	103	1.166 ± 0.005	0.750 ± 0.006	502.2	108.72	**108.68 ± 1.62**		
BMS1-VI	32	37	1.161 ± 0.004	0.755 ± 0.008	7.3	110.63	**108.31 ± 2.19**	**Outlier**	**2.02**
BMS1-VI-BIS	32	42	1.151 ± 0.007	0.759 ± 0.006	9.1	113.55	**111.64 ± 2.16**	**Age ok**	**1.94**
BMS1-2015-2a	52	96	1.161 ± 0.006	0.748 ± 0.006	1157.3	108.92	**108.90 ± 1.86**	**109.75 ± 1.33**	**1.22**
BMS1-2015-2b	52	73	1.162 ± 0.006	0.756 ± 0.006	1746.4	110.68	**110.66 ± 1.91**		
BMS1-E	60	88	1.160 ± 0.006	0.752 ± 0.007	1026.9	110.19	**110.15 ± 2.01**	**Age ok**	**1.83**
BMS1-2015-1	70	75	1.163 ± 0.005	0.763 ± 0.006	1195.7	112.34	**112.32 ± 1.75**	**Age ok**	**1.56**
BMS1-V	78	75	1.161 ± 0.004	0.759 ± 0.005	174.0	111.65	**111.56 ± 1.50**	**Age ok**	**1.34**
BMS1-IV	108	72	1.160 ± 0.004	0.757 ± 0.006	113.6	111.30	**111.15 ± 1.57**	**Age ok**	**1.41**
BMS1-3	114	43	1.158 ± 0.003	0.758 ± 0.005	647.7	111.98	**111.95 ± 1.48**	**Age ok**	**1.32**
BMS1-D I	119	107	1.152 ± 0.005	0.752 ± 0.007	1402.0	111.44	**111.43 ± 2.09**	**111.37 ± 1.34**	**1.20**
BMS1-D II	119	124	1.163 ± 0.004	0.759 ± 0.006	1765.4	111.33	**111.32 ± 1.74**		
BMS1-C I	124	36	1.151 ± 0.004	0.762 ± 0.007	10.6	114.29	**112.66 ± 2.07**	**112.46 ± 1.78**	**1.58**
BMS1-C II	124	38	1.134 ± 0.003	0.770 ± 0.008	2.3	120.02	**111.91 ± 3.48**		
BMS1-2	129	10	1.164 ± 0.004	0.775 ± 0.007	86.4	115.10	**114.91 ± 2.05**	**Outlier**	**1.79**
BMS1-III	139	39	1.158 ± 0.004	0.758 ± 0.006	537.1	112.06	**112.03 ± 1.64**	**Age ok**	**1.46**
BMS1-II	160	29	1.154 ± 0.005	0.766 ± 0.007	18.1	114.70	**113.74 ± 2.16**	**Age ok**	**1.90**
BMS1-B	209	43	1.156 ± 0.005	0.757 ± 0.009	138.1	112.03	**111.89 ± 2.51**	**Age ok**	**2.24**
BMS1-I	254	74	1.157 ± 0.004	0.759 ± 0.005	676.6	112.31	**112.27 ± 1.45**	**Age ok**	**1.29**
BMS1-1	288	41	1.160 ± 0.004	0.766 ± 0.004	771.3	113.70	**113.68 ± 1.34**	**Age ok**	**1.17**
BMS1-A	293	119	1.157 ± 0.003	0.760 ± 0.008	1249.5	112.67	**112.66 ± 2.00**	**Age ok**	**1.78**

Table 1. BMS1 U-Th age data. Depths are measured from the top of the stalagmite. U-Th ratios and ages are followed by the relative 2σ uncertainty. Corrected ages are calculated using the ^{230}Th and ^{234}U decay constants of Cheng et al. (2013) and equation 1 in Hellstrom (2006), assuming an initial $^{230}Th/^{232}Th = 0.25 \pm 0.08$. $(^{230}Th/^{232}Th)_{initial}$ was calculated following the stratigraphical constraint of Hellstrom (2006); although different from the conventionally used upper crust value, its value is in the range reported in literature (Hellstrom et al., 2006) and similar to the $(^{230}Th/^{232}Th)_{initial}$ in Drysdale et al. (2005). The associated error (2σ) of the corrected ages is lower than 2.3% (2.2 ka). Ages at the same depth have been averaged; two outliers have been identified after statistical analyses (see S.I.).

References

Allen, J.R.M., Huntley, B., 2009. Last Interglacial palaeovegetation, palaeoenvironments and chronology: a new record from Lago Grande di Monticchio, southern Italy. Quaternary Science Reviews 28, 1521-1538.

Banderas, R., Álvarez-Solas, J., Montoya, M., 2012. Role of CO_2 and Southern Oceans in glacial abrupt climate change. Climate of the Past 8, 1011-1021.

Bazin, L., Landais, A., Lemieux-Dudon, B., Toyé Mahamadou Kele, H., Veres, D., Parrenin, F., Martinerie, P., Ritz, C., Capron, E., Lipenkov, V., 2013. An optimized multi-proxy, multi-site Antarctic ice and gas orbital chronology (AICC2012): 120-800 ka. Climate of the Past 9, 1715-1731.

Boch, R., Cheng, H., Spötl, C., Edwards, R.L., Wang, X., Häuselmann, P., 2011. NALPS: a precisely dated European climate record 120–60 ka. Climate of the Past 7, 1247-1259.

Buizert, C., Cuffey, K.M., Severinghaus, J.P., Baggenstos, D., Fudge, T.J., Steig, E.J., Markle, B.R., Winstrup, M., Rhodes, R.H., Brook, E.J., Sowers, T.A., Clow, G.D., Cheng, H., Edwards, R.L., Sigl, M., McConnell, J.R., Taylor, K.C., 2015. The WAIS Divide deep ice core WD2014 chronology. Part 1: Methane synchronization (68–31 ka BP) and the gas age–ice age difference. Climate of the Past 11, 153-173.

Capron, E., Landais, A., Chappellaz, J., Schilt, A., Buiron, D., Dahl-Jensen, D., Johnsen, S.J., Jouzel, J., Lemieux-Dudon, B., Loulergue, L., Leuenberger, M., Masson-Delmotte, V., Meyer, H., Oerter, H., Stenni, B., 2010. Millennial and sub-millennial scale climatic variations recorded in polar ice cores over the last glacial period. Climate of the Past 6, 345-365.

Capron, E., Landais, A., Chappellaz, J., Buiron, D., Fischer, H., Johnsen, S. J., Jouzel, J., Leuenberger, M., Masson-Delmotte, V., Stocker, T. F., 2012. A global picture of the first abrupt climatic event occurring during the last glacial inception. Geophysical Research Letters 39, L15703.

Cheng, H., Lawrence Edwards, R., Shen, C.-C., Polyak, V. J., Asmerom, Y., Woodhead, J., Hellstrom, J., Wang, Y., Kong, X., Spötl, C., Wang, X., Calvin Alexander, E., 2013. Improvements in ^{230}Th dating, ^{230}Th and ^{234}U half-life values, and U–Th isotopic measurements by multi-collector inductively coupled plasma mass spectrometry. Earth and Planetary Science Letters 371-372, 82-91.

Culver, D.C., White, W.B., 2005. Encyclopedia of caves. Elsevier Amsterdam (The Netherlands).

Dansgaard, W., 1964. Stable isotopes in precipitation. Tellus 16, 436-468.

Dansgaard, W., Johnsen, S.J., Clausen, H.B., Dahl-Jensen, D., Gundestrup, N.S., Hammer, C.U., Hvldberg, C.S., Steffensen, J.P., Sveinbjornsdottir, A.E., Jouzel, J., Bond, G., 1993. Evidence for general instability of past climate from a 250-kyr ice-core record. Nature 364, 218-220.

Deininger, M., Fohlmeister, J., Scholz, D., and Mangini, A., 2012. Isotope disequilibrium effects: The influence of evaporation and ventilation effects on the carbon and oxygen isotope composition of speleothems–A model approach. Geochimica et Cosmochimica Acta, 96, 57-79.

Dokken, T. M., Nisancioglu, K. H., Li, C., Battisti, D. S., Kissel, C., 2013. Dansgaard-Oeschger cycles: Interactions between ocean and sea ice intrinsic to the Nordic seas. Paleoceanography 28 (3), 491-502.

Dredge, J., Fairchild, I.J., Harrison, R.M., Fernandez-Cortes, A., Sanchez-Moral, S., Jurado, V., Gunn, J., Smith, A., Spötl, C., Mattey, D., 2013. Cave aerosols: distribution and contribution to speleothem geochemistry. Quaternary Science Reviews 63, 23-41.

Drysdale, R. N., Zanchetta, G., Hellstrom, J., Maas, R., Fallick, A., Pickett, M., Cartwright, I., and Piccini, L., 2006. Late Holocene drought responsible for the collapse of Old World civilizations is recorded in an Italian cave flowstone: Geology, 34, 2, 101-104.

Drysdale, R.N., Hellstrom, J.C., Zanchetta, G., Fallick, A.E., Sanchez Goni, M.F., Couchoud, I., McDonald, J., Maas, R., Lohmann, G., Isola, I., 2009. Evidence for obliquity forcing of glacial Termination II. Science 325, 1527-1531.

Drysdale, R.N., Paul, B.T., Hellstrom, J.C., Couchoud, I., Greig, A., Bajo, P., Zanchetta, G., Isola, I., Spötl, C., Baneschi, I., Regattieri, E., Woodhead, J.D., 2012. Precise microsampling of poorly laminated speleothems for U-series dating. Quaternary Geochronology 14, 38-47.

Drysdale, R.N., Zanchetta, G., Hellstrom, J., Fallick, A.E., Zhao, J., 2005. Stalagmite evidence for the onset of the Last Interglacial in southern Europe at 129 ± 1 ka. Geophysical Research Letters 32, L24708.

Drysdale, R.N., Zanchetta, G., Hellstrom, J.C., Fallick, A.E., McDonald, J., Cartwright, I., 2007. Stalagmite evidence for the precise timing of North Atlantic cold events during the early last glacial. Geology 35, 77-80.

Duliński, M., Rozanski, K., 1990. Formation of 13C12C isotope ratios in speleothems: a semi-dynamic model. Radiocarbon, 32, 1, 7-16

Fairchild, I.J., Smith, C.L., Baker, A., Fuller, L., Spötl, C., Mattey, D., McDermott, F., E.I.M.F, 2006. Modification and preservation of environmental signals in speleothems. Earth-Science Reviews 75, 105-153.

Fleitmann, D., Cheng, H., Badertscher, S., Edwards, R., Mudelsee, M., Göktürk, O., Fankhauser, A., Pickering, R., Raible, C., Matter, A., 2009. Timing and climatic impact of Greenland interstadials recorded in stalagmites from northern Turkey. Geophysical Research Letters 36, L19707.

Franke, H., 1965. The theory behind stalagmite shapes. Studies in Speleology 1, 89-95.

Frisia, S., 2015. Microstratigraphic logging of calcite fabrics in speleothems as tool for palaeoclimate studies. International Journal of Speleology 44, 1-16.

Genty, D., Blamart, D., Ouahdi, R., Gilmour, M., Baker, A., Jouzel, J., Sandra, V.E., 2003. Precise dating of Dansgaard– Oeschger climate oscillations in western Europe from stalagmite data. Nature 42, 833-837.

Govin, A., Capron, E., Tzedakis, P. C., Verheyden, S., Ghaleb, B., Hillaire-Marcel, C., St-Onge, G., Stoner, J. S., Bassinot, F., Bazin, L., Blunier, T., Combourieu-Nebout, N., El Ouahabi, A., Genty, D., Gersonde, R., Jimenez-Amat, P., Landais, A., Martrat, B., Masson-Delmotte, V., Parrenin, F., Seidenkrantz, M.S., Veres, D., Waelbroeck, C., Zahn, R., 2015. Sequence of events from the onset to the demise of the Last Interglacial: Evaluating strengths and limitations of chronologies used in climatic archives. Quaternary Science Reviews 129, 1-36.

GRIP, Greenland Ice Core Projects Members, 1993. Climate instability during the last interglacial period recorded in the GRIP ice core. Nature 364, 203-207.

Grootes, P.M., Stulver, M., White, J.W.C., Johnsen, S., Jouzel, J., 1993. Comparison of oxygen isotope records from the GISP2 and GRIP Greenland ice cores. Nature 366, 552-554.

Hellstrom, J., 2003. Rapid and accurate U/Th dating using parallel ion-counting multi-collector ICP-MS. Journal of Analytical Atomic Spectrometry 18, 1346-1351.

Hellstrom, J., 2006. U–Th dating of speleothems with high initial 230Th using stratigraphical constraint: Quaternary Geochronology 1(4), 289–295. doi:10.1016/j.quageo.2007.01.004.

Henderson, G.M., 2006. Climate. Caving in to new chronologies. Science 313, 620-622.

Hendy, C. H., 1971. The isotopic geochemistry of speleothems-I. The calculation of the effects of different modes of formation on the isotopic composition of speleothems and their applicability as palaeoclimatic indicators. Geochimica et Cosmochimica Acta 35, 801-824.

Kaufmann, G., Dreybrodt, W., 2004. Stalagmite growth and palaeo-climate: an inverse approach. Earth and Planetary Science Letters 224, 529-545.

Kindler, P., Guillevic, M., Baumgartner, M., Schwander, J., Landais, A., Leuenberger, M., 2014. Temperature reconstruction from 10 to 120 kyr b2k from the NGRIP ice core. Climate of the Past 10, 887-902.

Krklec, K., Domínguez-Villar, D., 2014. Quantification of the impact of moisture source regions on the oxygen isotope composition of precipitation over Eagle Cave, central Spain. Geochimica et Cosmochimica Acta 134, 39-54.

Lachniet, M.S., 2009. Climatic and environmental controls on speleothem oxygen-isotope values. Quaternary Science Reviews 28, 412-432.

Martin-Puertas, C., Brauer, A., Wulf, S., Ott, F., Lauterbach, S., Dulski, P., 2014. Annual proxy data from Lago Grande di Monticchio (southern Italy) between 76 and 112 ka: new chronological constraints and insights on abrupt climatic oscillations. Climate of the Past 10, 2099-2114.

McDermott, F., 2004. Palaeo-climate reconstruction from stable isotope variations in speleothems: a review. Quaternary Science Reviews, 23, 901-918.

Moreno, A., Svensson, A., Brooks, S., Connor, S., Engels, S., Fletcher, W.J., Genty, D., Heiri, O., Labuhn, I., Persoiu, A., Peyron, O., Sadori, L., Valero-Garces, B., Wulf, S., Zanchetta, G., 2014. A compilation of Western European terrestrial records 60-8 ka BP: towards an understanding of latitudinal climatic gradients. Quaternary Science Reviews 106, 167-185.

Mühlinghaus, C., Scholz, D., and Mangini, A., 2009. Modelling fractionation of stable isotopes in stalagmites. Geochimica et Cosmochimica Acta, 73, 24, 7275-7289.

NGRIP, North Greenland Ice Core Project Members, 2004. High-resolution record of Northern Hemisphere climate extending into the last interglacial period. Nature 431, 147-151.

Rasmussen, S.O., Bigler, M., Blockley, S.P., Blunier, T., Buchardt, S.L., Clausen, H.B., Cvijanovic, I., Dahl-Jensen, D., Johnsen, S.J., Fischer, H., Gkinis, V., Guillevic, M., Hoek, W.Z., Lowe, J.J., Pedro, J.B., Popp, T., Seierstad, I.K., Steffensen, J.P., Svensson, A.M., Vallelonga, P., Vinther, B.M., Walker, M.J.C., Wheatley, J.J., Winstrup, M., 2014. A stratigraphic framework for abrupt climatic changes during the Last Glacial period based on three synchronized Greenland ice-core records: refining and extending the INTIMATE event stratigraphy. Quaternary Science Reviews 106, 14-28.

Regattieri, E., Zanchetta, G., Drysdale, R.N., Isola, I., Hellstrom, J.C., Roncioni, A., 2014. A continuous stable isotope record from the penultimate glacial maximum to the Last Interglacial (159–121ka) from Tana Che Urla Cave (Apuan Alps, central Italy). Quaternary Research 82, 450-461.

Scholz, D., Hoffmann, D.L., Hellstrom, J., Bronk Ramsey, C., 2012. A comparison of different methods for speleothem age modelling. Quaternary Geochronology 14, 94-104.

Svensson, A., Andersen, K., Bigler, M., Clausen, H., Dahl-Jensen, D., Davies, S., Johnsen, S., Muscheler, R., Parrenin, F., Rasmussen, S.O, 2008. A 60 000 year Greenland stratigraphic ice core chronology. Climate of the Past 4, 47-57.

Veres, D., Bazin, L., Landais, A., Toyé Mahamadou Kele, H., Lemieux-Dudon, B., Parrenin, F., Martinerie, P., Blayo, E., Blunier, T., Capron, E., 2013. The Antarctic ice core chronology (AICC2012): an optimized multi-parameter and multi-site dating approach for the last 120 thousand years. Climate of the Past Discussions 9.4, 1733-1748.

Voelker, A., 2002. Global distribution of centennial-scale records for Marine Isotope Stage (MIS) 3: a database. Quaternary Science Reviews 21, 1185-1212.

WAIS, 2015. Precise interpolar phasing of abrupt climate change during the last ice age. Nature 520, 661-665.

Wang, Y.J., Cheng, H., Edwards, R.L., An, Z.S., Wu, J.Y., Shen, C.C., Dorale, J.A., 2001. A high-resolution absolute-dated late Pleistocene Monsoon record from Hulu Cave, China. Science 294, 2345-2348.

Wolff, E.W., Chappellaz, J., Blunier, T., Rasmussen, S.O., Svensson, A., 2010. Millennial-scale variability during the last glacial: The ice core record. Quaternary Science Reviews 29, 2828-2838.

Zhang, X., Lohmann, G., Knorr, G., Purcell, C., 2014. Abrupt glacial climate shifts controlled by ice sheet changes. Nature 512, 290-294.